

## Research Paper

**Cite this article:** Kazemi F, Mohanna F, Ahmadi-Shokouh J (2018). Detection of biological abnormalities using a near-field microwave microscope. *International Journal of Microwave and Wireless Technologies* **10**, 933–941. <https://doi.org/10.1017/S1759078718000752>

Received: 23 January 2018

Revised: 7 April 2018

Accepted: 12 April 2018

First published online: 21 May 2018

### Key words:

Biological abnormalities; microwave imaging; skin cancer; subcutaneous masses

### Author for correspondence:

F. Mohanna, E-mail: [F\\_mohanna@ece.usb.ac.ir](mailto:F_mohanna@ece.usb.ac.ir)

# Detection of biological abnormalities using a near-field microwave microscope

Fatemeh Kazemi, Farahnaz Mohanna and Javad Ahmadi-Shokouh

Faculty of Electrical and Computer Engineering, University of Sistan and Baluchestan, Zahedan, Iran

Microwave and millimeter-wave reflectometry is one of the potential techniques for the diagnosis and detection of biological abnormalities, such as subcutaneous masses or cancerous tumors in human body. In this paper, a high-quality microwave sensor based on planar microstrip resonator is designed, fabricated, and successfully tested with different kinds of biological samples. The proposed sensor has unique properties such as small size, simple fabrication, non-contact with a sample, excellent de-coupling from surroundings, and high microwave power is directly coupled into the tissue. Two experiments are performed for the detection of visible and hidden “lipoma” (fat masses), and minimum size of “lipoma” that is diagnosed by the sensor is obtained as well. In this regard, a two-dimensional image of hidden “lipomas” with amplitude contrast about 30 dB and frequency shifts contrast about 60 MHz at a  $\lambda/10$  (at 13.5 GHz) stand-off distance is provided. Finally, a measurement scenario for the detection of skin cancer based on the artificial model using different layers of raw chicken with different water content is described. Results show that the proposed microscope is easy to fabricate and provide a low-cost solution for fast and accurate skin cancer detection.

## Introduction

Near-field microwave microscopy is widely used in non-destructive evaluation and characterization of materials, e.g. dielectric and metal structures [1–5], biological samples [6–8], and critical parts of buildings and constructions [9, 10]. The advantages of microwave reflectometry include low-power, real-time, and non-contact operation with high-sensitivity and high-resolution imaging of the target [11–14].

Nowadays, microwave imaging is an attractive alternative modality for early-stage characterization of biological abnormalities such as detection of tumors in breast cancer [15–17], skin cancer, and skin burn injuries [18–24]. The procedure is comfortable, and the clinical system cost is a small fraction of the cost of an X-ray system, making it affordable for widespread screening. The procedure poses no safety hazards, and the potential is significant for detecting very small tumors in the early stages of development [25]. The early-tumor detection principle is based on the analysis of the differences in the dielectric properties between the healthy and malignant tissues [26]. For example, the dielectric properties of skin are directly related to the parameters such as water, sodium, and protein content, which differ between normal skin and benign and malignant lesions. The water content for malignant tumor is about 20% higher than normal skin [27]. This difference in water content is expected to be readily detected in microwave measurements. The reflection properties that are measured are directly influenced by the dielectric properties of the material being studied [28]. Additionally, different types of sensors may be used for microwave reflectometry, which expand the potential for material characterization including detection of skin abnormalities.

In this paper, a microwave imaging system for the characterization of skin abnormalities is proposed. For this purpose, a microwave sensor based on planar microstrip line at 13.5 GHz is designed. Unique advantages of two-dimensional (2D) waveguide structures such as microstrip lines as microwave sensors are as follow: (a) by using different dielectric constants and substrate thicknesses, various angles of taper and different apertures, the resolution of the sensor can be engineered; (b) to produce miniature parallel and compact sensors, this sensor can be integrated with silicon micro-machined parts.

After the design and fabrication of a microwave sensor, the performance of the proposed sensor is evaluated using biological materials such as different tissues of raw chicken including skin, fat, and muscle (with different electromagnetic properties). Then, a measurement scenario for the detection of biological abnormalities using fat masses along the muscle tissue (as “lipoma”) is defined. For this purpose, two experiments are performed to measure the resolution of the sensor for the detection of hidden and visible “lipoma”. Moreover, for authentication of experimental results, an image of hidden “lipomas” (with different size and space) below the skin is obtained.

Finally, the capability of proposed sensor for the detection of skin cancer using an artificial skin model is studied. In this experiment, microwave properties of the healthy skin, malignant

tumors, and benign lesions are modeled using layers of raw chicken skin with different water content.

The rest of the paper is organized as follows. In “Microwave sensor characteristics” section, design principles of a microwave sensor are explained and the operation principle and experimental procedure used in microwave measurements are discussed in “Operation principles and background theory” and “Experimental set-up and procedure” sections, respectively. In the next section, surface and subsurface characterization of “lipomas” are measured. Then, a microwave image of hidden “lipomas” with a different size and space below the skin is obtained. Also, a measurement scenario for the detection of skin cancer is described. Finally, some concluding remarks are given in “Conclusion” section.

**Microwave sensor characteristics**

A microwave sensor for surface and subsurface imaging is designed based on two key points: (1) to have a sensor with high sensitivity, quality factor of the sensor should be high as much as possible. For this goal, a cavity resonator in the sensor structure is used to minimize the reflection coefficient; (2) to improve the image resolution as much as possible, the sensor tip should be sharpest.

Geometry of a microwave sensor with  $\lambda/2$  length of a 50  $\Omega$  open-circuited microstrip line is shown in Fig. 1. This sensor is design for the resonance at 13.5 GHz. The reason for choosing this frequency is to compromise between the penetration depth of the sensor and the resolution of the raw images. In other words, because the purpose is imaging of the subcutaneous masses, a frequency that can detect the hidden objects in the images with acceptable resolution and without any damage to the tissue is selected. The practical principle of a sensor using microstrip resonator is described in [29, 30]. Substrate of this structure is RT/duroid 5880 ( $\epsilon_r = 2.2$ ,  $\tan(\delta) = 0.0009$ ) with a thickness of 0.8 mm.

Design of the sensor is performed in two steps. First, the effect of two important parameters including tip sharpness ( $\alpha$ ) and size of the coupling gap on the sensor performance is numerically investigated using Ansoft HFSS software. The sharp angle ( $\alpha$ ) and the coupling gap size in order to have minimum of the return loss are achieved 11.2° and 0.2 mm, respectively. Final dimensions of the sensor are shown in Table 1. Quality factor of the sensor is obtained 5270.

In the second step of sensor design, for reducing the side lobe level and focusing energy on the tip as much as possible, substrate and ground plane at the sensor tip is cut with different angles.

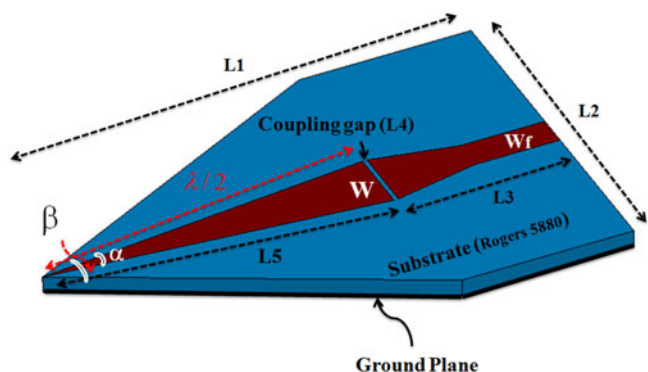


Fig. 1. Geometry of a microwave sensor.

Table 1. Dimensions (mm) of the sensor

$W$	$W_f$	$L_1$	$L_2$	$L_3$	$L_4$	$L_5$	$\alpha$
3.1	1.5	24	16	8	0.2	15.8	11.2°

Simulation results show that the angle ( $\beta$ ) to have the highest field strength at the sensor tip is 53.4°. This cutting does not have effect on the quality factor of the sensor and only shifts slightly the resonant frequency. But near-field pattern of the sensor is significantly oriented on the sensor tip direction as shown in Fig. 2. Photograph of the manufactured sensor, simulation, and measurement results of the sensor’s reflection coefficient are shown in Fig. 3.

**Operation principles and background theory**

When the microwave sensor is placed in the vicinity of a material under test (MUT), dielectric properties of MUT affect the quality factor ( $Q$ ) and the resonant frequency ( $f_r$ ) of the sensor (Fig. 4 (a)). These changes depend on the electromagnetic properties as well as the effective area of the sensor tip ( $A_{eff}$ ,  $A_p$ ) and the distance between MUT and the sensor tip ( $d_s$ ). If the effective area of the sensor tip and distance between MUT and the tip is fixed, the sensor can scan the MUT and variations in the MUT’s electromagnetic properties can be recorded [30].

The electromagnetic properties of an MUT are a function of free carrier concentration, permeability, and permittivity. In human and biological tissues, the amounts of humidity and ionic species have a significant impact on its conductivity. Near-field microwave sensor can map these parameters and their density variations, which have effect on the permittivity [30]. There are different signal detection methods for monitoring the electromagnetic properties of a material using a near-field sensor. As shown in Fig. 4(a), when the operation frequency at  $f_{cal}$  (as calibration frequency) is fixed, the change in amplitude and phase of the reflection coefficient can be monitored. Calibration frequency ( $f_{cal}$ ) is usually selected by the frequency where the reflection coefficient of the sensor has the maximum change for a given range of parameters in a material. Since the resonant frequency varies during the scan of material, the frequency shift ( $\Delta f$ ) also can be detected.

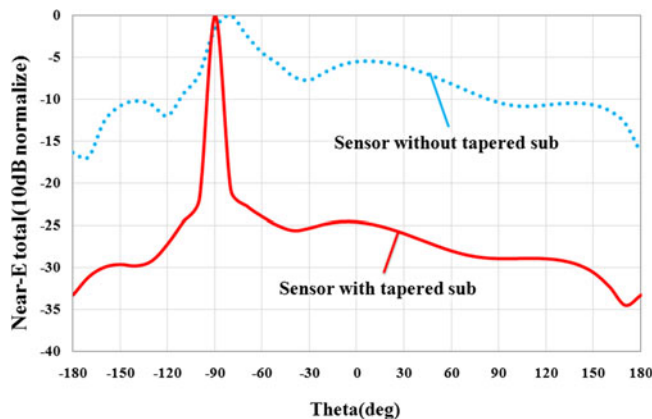


Fig. 2. Rectangular near-field pattern of the sensor at 13.5 GHz (H-plane).

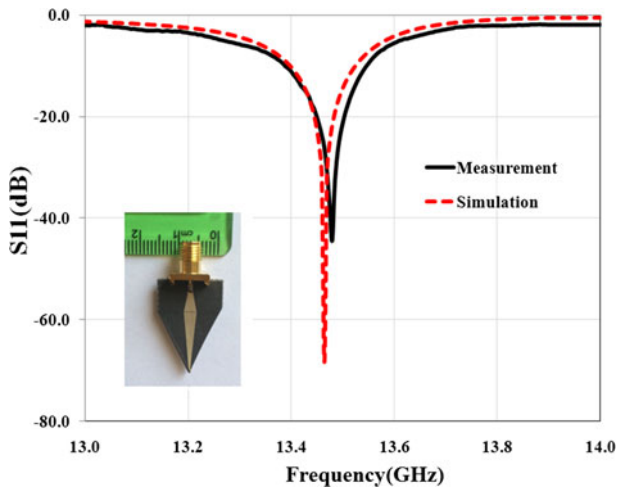


Fig. 3. Reflection coefficient of the sensor and photograph of the manufactured sensor.

As shown in Fig. 4(a), given a change in the reflection coefficient  $\Delta S_{11}$  per a small change of  $\Delta d_s$  in the distance between an MUT and the sensor tip, we can only detect  $\Delta S_{11}$  if it is equal to or larger than the combined noise produced by the detector. The signal-to-noise ratio is an arbitrary requirement that it can be improved by using synchronous detection methods. If relationship between  $\Delta S_{11}$  and  $\Delta f$  in Fig. 4(a) is defined by:

$$\Delta S_{11} \approx \left. \frac{\Delta S_{11}}{\Delta f} \right|_{f_{cal}} \times \Delta f. \tag{1}$$

Then  $(\Delta S_{11}/\Delta f)_{f_{cal}}$  is defined as the sensitivity of the near-field sensor at  $f_{cal}$  and can be noted by  $S_{cal}$ . Moreover, the minimum-detectable signal (MDS) can be defined as the smallest change in the input that produces an output ( $\Delta V_{out} = \Delta S_{11} V_{in}$ ) equal to the rms value of the noise  $V_{nrms}$ . Also, if  $\Delta S_{11}/\Delta f$  is written as  $\Delta S_{11}/\Delta f = \Delta S_{11}/\Delta d_s \times \Delta d_s/\Delta f$  then we can write [31]:

$$\Delta S_{11} = \frac{V_{nrms}}{V_{in}}, \tag{2}$$

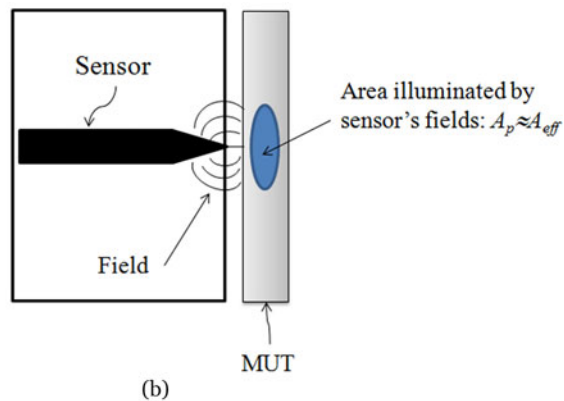
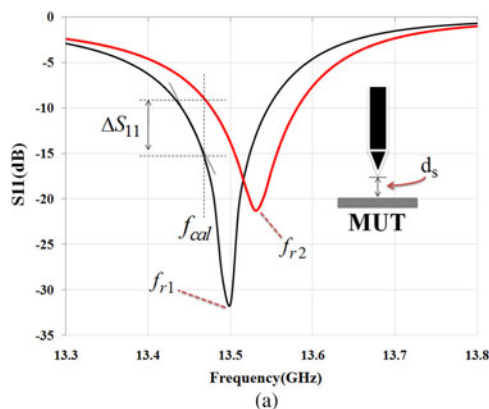


Fig. 4. (a) Resonant frequency and amplitude of the reflection coefficient is changed when the sensor is placed in front of the MUT. (b) Interaction between near-field sensor and MUT.

and

$$MDS = \Delta d_s = \frac{V_{nrms}/V_{in}}{S_{cal} S_{d_s}}. \tag{3}$$

Here  $S_{d_s}$  is  $\Delta d_s/\Delta f$  and  $\Delta d_s$  is the smallest change in the stand-off distance. Equation (3) clearly shows that by maximizing of  $S_{d_s}$  and  $S_{cal}$ , the MDS will be improved.  $S_{cal}$  is related to the quality factor of the near-field sensor, while  $S_{d_s}$  is determined by the interaction between sensor and MUT.

Interaction between near-field sensor and MUT is shown in Fig. 4(b). The field patterns at the surface of the MUT are spread over an area denoted by  $A_{eff} \approx A_p$ , where  $A_p$  is the physical area of the sensor tip and  $A_{eff}$  is an effective interaction area [31]. It is very important to differentiate between variations in the distance and changes in the electromagnetic properties of the MUT. In practice both the MUT conductivity and distance between the sensor and the MUT will change during its scan. Fortunately, effect of the variations in distance appears exponentially on the sensor’s output while the MUT’s non-uniformity usually occurs over larger length scales.

We modeled the strip-line resonator (open-circuit transmission line) by a series RLC circuit near its resonance frequency (Fig. 5(a)). When an MUT is placed near the tip, its electromagnetic properties are coupled to the RLC circuit through a coupling capacitor. For simplicity, dielectric MUTs are modeled in Fig. 5 (b). In these figures,  $R_p$ ,  $L_p$  and  $C_p$  are the intrinsic circuit parameters of the strip-line resonator;  $C_c$  models the coupling capacitance of the air gap between a tip and an MUT;  $L_{MUT}$ ,  $C_{MUT}$  and  $R_{MUT}$  model the microwave properties of an MUT. The resonant frequency shifts in the presence of an MUT near a sensor tip. From these circuit models, it is clear that a shift in resonant frequency depends on both complex conductivities of the MUT and on the stand-off distance [32].

If the coupling capacitance  $C_c$  in Fig. 5(b) is defined by:

$$C_c = \frac{\epsilon_0 A_{eff}}{d_s}, \tag{4}$$

then we can calculate  $S_{d_s}$  as:

$$S_{d_s} = \frac{\epsilon_0 A_{eff} f_0}{d_s (C_p d_s + \epsilon_0 A_{eff})}. \tag{5}$$

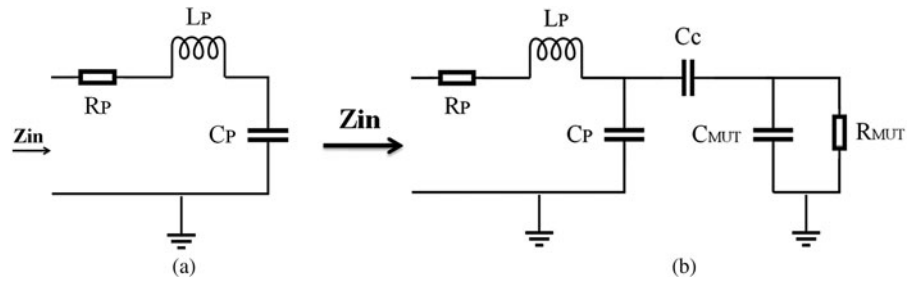


**Fig. 5.** (a) Series of lumped RLC models of a microwave sensor. (b) Circuit model in the presence of a dielectric MUT.

For typical values of a sensor ( $A_{eff} \approx A_p \approx 4 \times 10^{-4} \text{ cm}^2$ ,  $d_s = 2 \text{ mm}$ ,  $f_0 = 13.5 \text{ GHz}$ ,  $Q = 5270$ ,  $C_p = 7.3 \text{ pF}$ ,  $C_c = 12 \text{ pF}$ )  $S_{ds}$  becomes:

$$S_{ds} = \frac{8.85 \times 10^{-14} \times 4 \times 10^{-8} \times 13.5 \times 10^9}{2 \times 10^{-3}(7.3 \times 10^{-12} \times 2 \times 10^{-3} + 8.85 \times 10^{-14} \times 4 \times 10^{-4})} = 3.2575 \times 10^6.$$

It should be noted that  $S_{ds}$  has an inverse relationship with distance square between a sensor and an MUT ( $/d_s^2$ ). This means that dependency will be exponential if a sensor is very near to an MUT.

Assuming that the resonator is matched to the characteristic impedance of the feed-line at calibration frequency,  $S_{cal}$  is calculated by [31]:

$$S_{cal} \approx s \frac{\sqrt{2}Q}{\omega_{cal}} \left(1 - \frac{\Delta\omega}{\omega_{cal}}\right), \tag{6}$$

where  $\omega = \omega_{cal} + \Delta\omega$  and  $\Delta\omega/\omega_{cal} < 1$  and  $s = -1$  if  $\omega < \omega_{cal}$  and  $s = +1$  if  $\omega > \omega_{cal}$ . Therefore, as we expect, the sensor sensitivity is directly proportional to its quality factor. For the near-field sensor in this study,  $S_{cal}$  is calculated  $4.4 \times 10^{-8}$ .

Using equations (5) and (6) in equation (3), we have:

$$MDS = \Delta d_s \approx \frac{V_{nrms}}{V_{in}} \frac{2\pi d_s(C_p d_s)}{Q(1 - \Delta f/f_{cal})\epsilon_0 A_{eff}}. \tag{7}$$

For typical values of  $S_{cal}$  and  $S_{ds}$  in equations (5) and (6), a numerical value of 0.75 mm is obtained for MDS. The circuit

approach that is used in defining the coupling capacitance is only an approximation and it does not account for the decay of electromagnetic fields near the tip. Our experimental set-up and procedure for microwave measurements are discussed in the next section.

### Experimental set-up and procedure

In this section, first, a simulation study is investigated by HFSS software to show the capability of the sensor for the diagnosis of different biological tissues. For this purpose, according to the experiments, the near-field sensor is placed in front of different tissues such as skin ( $\epsilon_r = 27.5-j16$  at 13.5 GHz), fat ( $\epsilon_r = 3.6-j0.6$  at 13.5 GHz), and muscle ( $\epsilon_r = 32.2-j25$  at 13.5 GHz). The dielectric values for different tissues were interpolated from the values given by Gabriel *et al.* [33]. As shown in Fig. 6(a), quality factor ( $Q$ ) and resonant frequency ( $f_r$ ) of the sensor are affected by the electromagnetic properties of the tissues. The simulation results in Fig. 6(a) show that the sensor will be able to detect the different tissues in the experiments. Moreover, the simulated near  $E$ -field (by HFSS) amplitude distribution at 2 mm at the frequency of 13.5 GHz in front of fat masses along the muscle tissue shows that the near-field focal area is substantially confined in space (Fig. 6(b)). Also, by increasing the distance, the energy focus reduces. Therefore, the stand-off distance to achieve the images with good resolution is 2 mm.

The experimental set-up used in this work is shown in Fig. 7. As mentioned, a microstrip resonator is used as a sensor that is connected to a 0.01–20 GHz vector network analyzer via an RF cable. The near-field sensor is fixed on the  $z$ -axis vertically to the MUT at  $0.1 \lambda$  stand-off distance away from the MUT and two-step motors move the MUT in the  $x$  and  $y$  directions. As

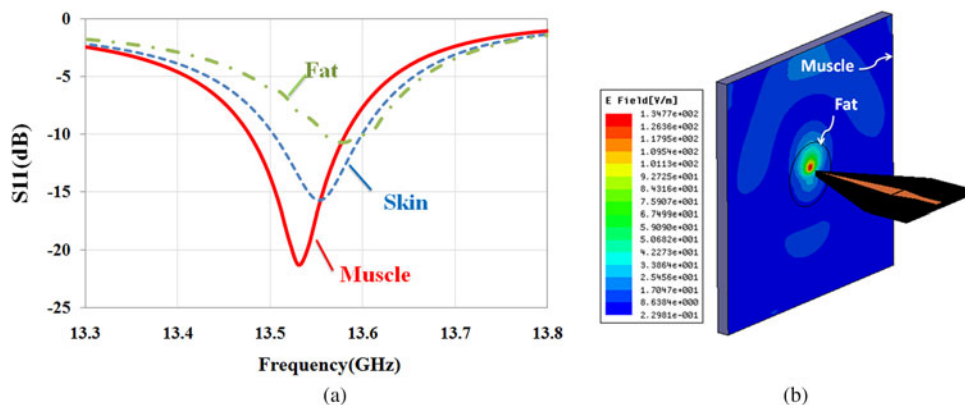


**Fig. 6.** (a) Reflection coefficient of the sensor in the presence of different biological tissues at 2 mm stand-off distance. (b)  $E$ -field amplitude at 2 mm stand-off distance in front of fat mass along the muscle tissue.

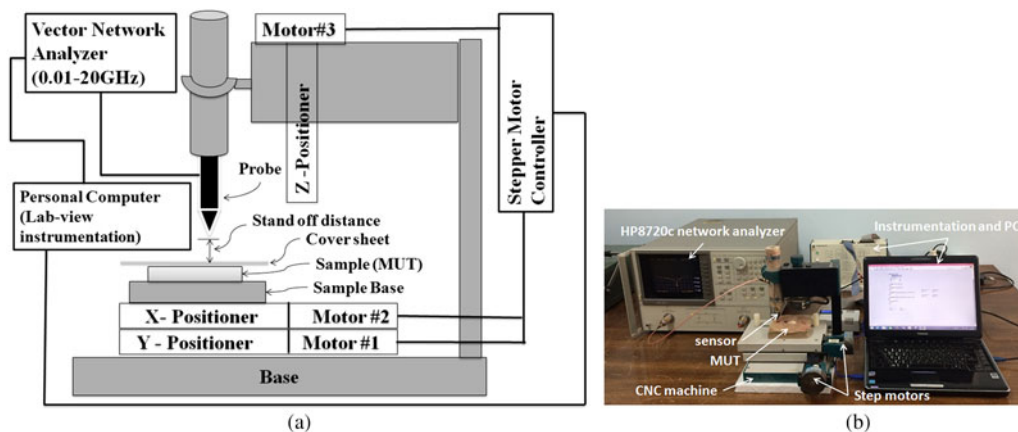


Fig. 7. (a) Schematic representation and (b) photograph of our experimental set-up.

mentioned before, since the sensor tip does not make contact with the MUT, the MUT’s surface can have a variety of characteristics, including being sticky or immersed in a dielectric fluid. Before measurement, the system is calibrated. To perform the calibration, distance between probe and MUT ( $d_s$ ) is changed to minimize the magnitude of the reflection coefficient. Then this distance is kept constant along our measurements (about 2 mm) and frequency of the minimum magnitude of  $S_{11}$  is considered as calibration frequency ( $f_{cal}$ ). During MUT scanning, magnitude of  $S_{11}$  at calibration frequency and frequency shift ( $\Delta f$ ) are recorded to detect the visible and hidden objects. Also, in our measurements, a National Instrument Data Acquisition with their Lab-View software is used to control the stepper motors and to acquire the measurement data. The movement step during all scanning measurements is 1 mm. Moreover, all experiments are carried out at room temperature (23 °C).

**Experimental results and discussion**

Since “lipoma” is a benign tumor composed of fat tissue and it is the most common benign form of soft-tissue tumor, in this section, a measurement scenario is defined based on the surface and subsurface detection of “lipoma”. Moreover, for results validation, an image of “lipomas” with different sizes and distances below a skin layer is obtained. Finally, our proposed sensor capability for skin cancer detection is studied using an artificial skin model.

**Surface and subsurface detection of “lipomas”**

In this section, in order to study the presented microscope features, resolution of the proposed near-field sensor for the diagnosis of “lipomas” is measured. Therefore, two experiments are applied. Initially, as shown in Fig. 8(a), four “lipomas” with a size of 20, 10, 5, and 3 mm are located orderly along the muscle tissue and the proposed sensor scans a vector of 85 mm length along them as well. Thickness of the tissues is considered about 2 mm for fat and muscle tissues and 1 mm for skin tissue. In all experiments, the tissues roughness is not considered, and to keep the stand-off distance between probe and tissues constant, a transparent plastic sheet (as cover sheet) is placed on the tissue. Subsequently, in each experiment, two parameters including the amplitude of reflection coefficient and the frequency shift are measured.

Measurement results of  $S_{11}$  in Fig. 8(b) show that the proposed sensor is able to detect the “lipomas” with sizes larger than 3 mm.

In the second experiment, for subsurface imaging, different sizes of fat masses are placed along the muscle tissues below the skin. As shown in Fig. 9(a), four “lipomas” with a size of 20, 10, 5, and 3 mm are located below the skin, respectively, and scanned by the proposed sensor. Fig. 9(b) shows the measurement results. Results show that the sensor is able to detect hidden “lipomas” at a minimum size of 5 mm. It is noted that in the medical research, masses that are grown larger than 5 mm is important for the diagnosis from cancerous tumor [34]. Therefore, the

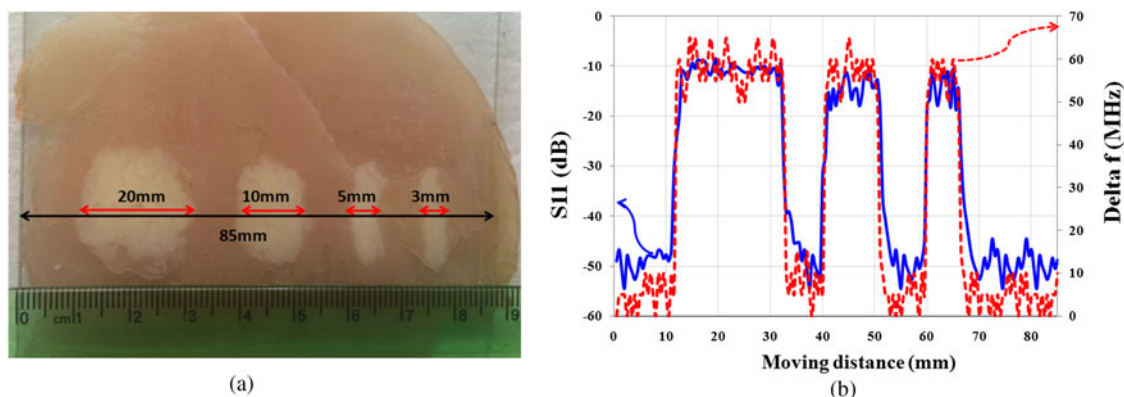
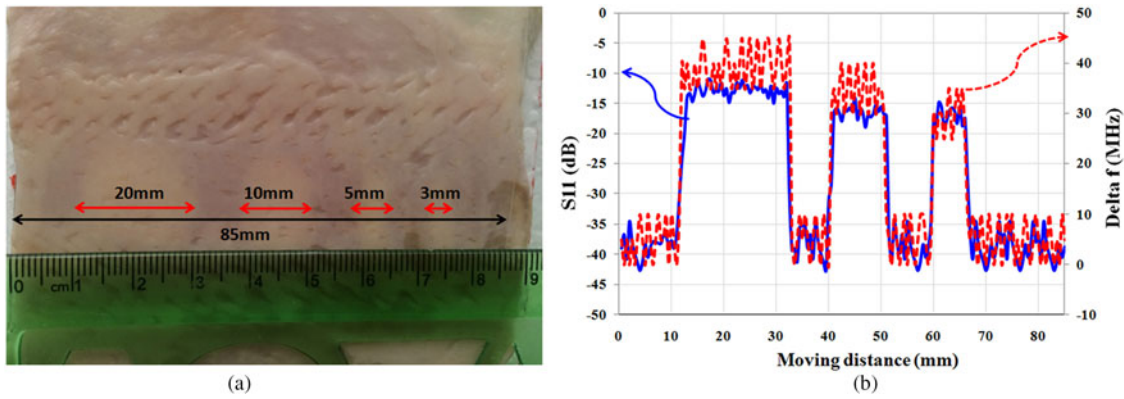


Fig. 8. (a) Photographs of “lipomas” with different sizes. (b) Magnitude of reflection coefficient and frequency shift ( $\Delta f$ ).



**Fig. 9.** (a) Photograph of “lipomas” with different sizes below skin layer. (b) Magnitude of reflection coefficient and frequency shift ( $\Delta f$ ).

proposed sensor is suitable for detecting subcutaneous masses and distinguishing them from the cancerous masses in the early stage.

**Image realization**

For results validation, an image of the hidden “lipomas” in different sizes and spaces is obtained. As shown in Figs 10(a) and 10(b),

the “lipomas” with different sizes are placed along the muscle tissues below a skin layer and the sensor scans a matrix of  $90 \times 90$  mm dimensions. The operation frequency is fixed at 13.5 GHz, where the image is obtained at 2 mm ( $\lambda/10$ ) imaging distance. As the results shown in Figs 10(c) and 10(d), high-quality raw images of “lipomas” below the skin are achieved with an amplitude contrast of about 15 dB and a frequency shift contrast of about 60 MHz.

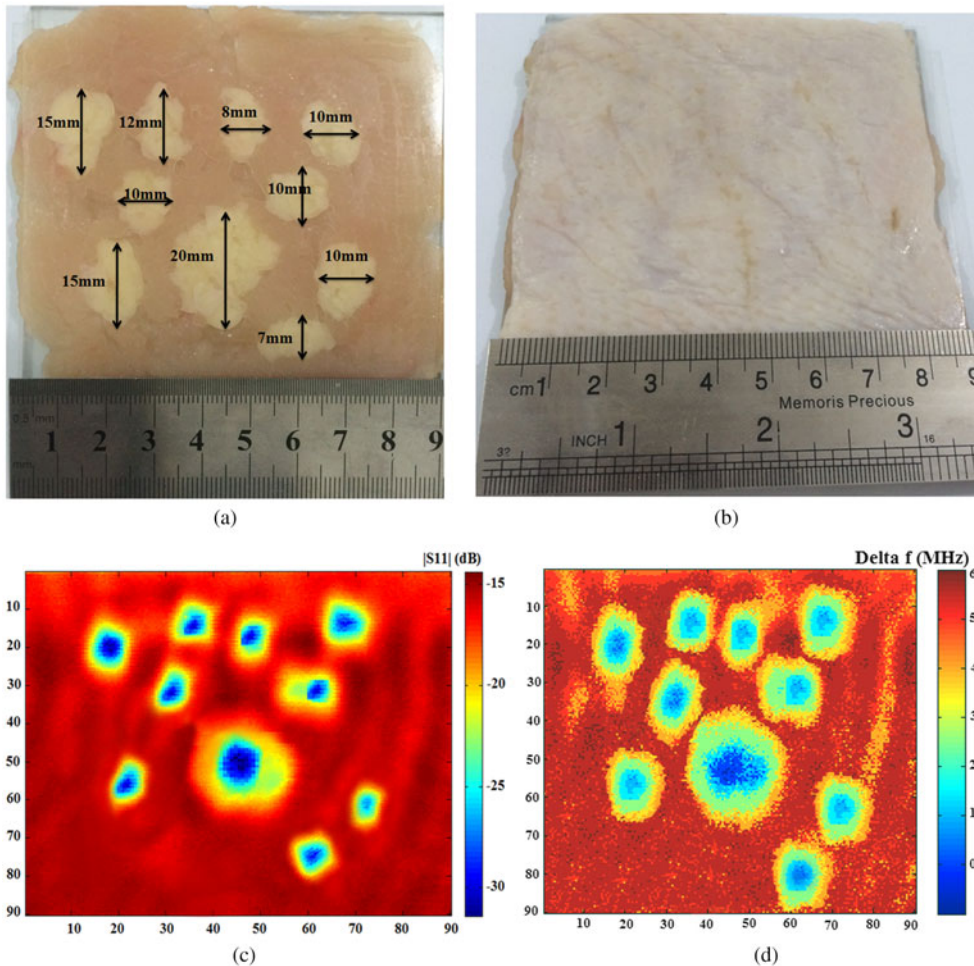


**Fig. 10.** Photograph of “lipomas” with different sizes, (a) without cover, (b) with cover by a layer of skin, and a microwave image from, (c) measurement of the  $S_{11}$  magnitude, (d) measurement of the frequency shift ( $\Delta f$ ).

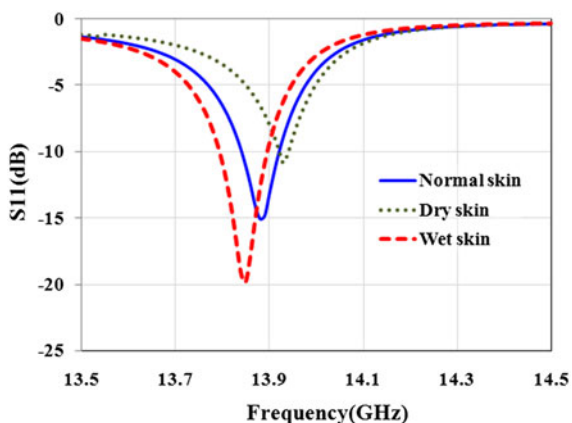


**Fig. 11.** Effect of water content in the skin on the magnitude and resonant frequency of reflection coefficient.

**Detection of skin cancer using an artificial skin model**

In all kinds of skin cancers, the amount of water content is increased, mostly, in the epidermis layer [27]. The water content of malignant lesions is about 20% higher than the normal skin. But, many benign lesions are drier than normal skin [35]. This difference in water content is expected to be readily detected in microwave measurements. At microwave frequencies, the dielectric properties of normal skin can be distinguished from those of lesions by measuring their reflection properties [28]. Previous studies [22–24] show that the microwave reflection contrast between the malignant tumor and healthy skin is approximately similar to that of dry and wet skin. Also, these studies diagnose the malignant tissue from normal tissue by the coaxial sensor with low contrast (1–3 dB) because of low coupling between the sensor and the tissues.

Before the experiment, a simulation was conducted to estimate the sensor’s ability to detect the skin with different water content. For this aim, sensor is placed in front of dry ( $\epsilon_r = 23.15 - j16.08$  at 13.5 GHz), normal ( $\epsilon_r = 27.5 - j16.11$  at 13.5 GHz), and wet ( $\epsilon_r = 29.64 - j17.26$  at 13.5 GHz) skin. Simulation results in Fig. 11 show that the sensor is able to diagnose the skin with different water content with high contrast.

In the experiment, microwave properties of the healthy skin, malignant tumors, and benign lesions are modeled using layers of raw chicken skin with different water content. For this purpose, a piece of raw chicken skin is placed in a tank of water for ~20 min (representing melanoma). Another piece of the skin is

placed in contact with air for 20 min (representing benign lesions). Moreover, a piece of normal skin (without contact with air and water) is considered as healthy skin. Then, as shown in Fig. 12(a), a few slices of melanomas and benign lesions are placed on the healthy skin and the sensor scans a vector along these tissues. This model is designed to represent skin cancer development at the early stages (<http://www.cancerresearchuk.org>, <http://www.skincancer.org/melanoma>) when only small, node-like tumors occur. Thickness of all layers of skin is about 1 mm and the size of skin slices (cancerous tumors) varies from ~5 mm ( $\lambda/4$ ) to 10 mm ( $\lambda/2$ ). The operation frequency is fixed at 13.5 GHz, where stand-off distance between sensor and skin is 2 mm ( $\lambda/10$ ). Measurement results in Fig. 12(b) show that the sensor could accurately detect malignant tumor with about 10 dB contrast in magnitude and 30 MHz contrast in frequency shifts from healthy skin and with about 30 dB contrast in magnitude and 60 MHz contrast in frequency shifts from benign lesions. It is noted that if dimensions of the sensor scale down, other types of skin cancer such as basal cell carcinoma and squamous cell carcinoma will be characterized with super resolution at millimeter waves.

**Conclusion**

In this paper, design, fabrication, and characterization of a microwave sensor for near-field microwave imaging of skin abnormalities are presented. The ability of the proposed sensor for imaging of different biological tissues such as skin, fat, and muscle is also studied. For this purpose, two experiments for surface and subsurface detection of “lipomas” are performed. First, for surface imaging, fat tissues of different sizes are placed along the muscle tissues. Second, for subsurface imaging, fat tissues of different sizes are placed along the muscle tissues below a layer of skin. Results show that the sensor is able to diagnose the visible and hidden “lipomas” of >5 mm in size. Finally, for results validation, a 2D microwave image of “lipomas” below the skin in different sizes and spaces is obtained. Results show that high-quality raw images of “lipomas” below the skin are achieved with an amplitude contrast of about 15 dB and a frequency shift contrast of about 60 MHz. Finally, a measurement scenario for the detection of skin cancer based on the artificial model using different layers of raw chicken with different water content is described. Results show that the proposed microscope is easy-to-fabricate, and provides a low-cost solution for fast and accurate skin cancer detection.

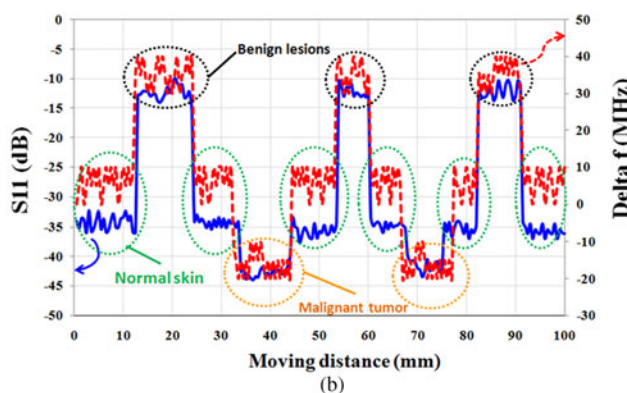
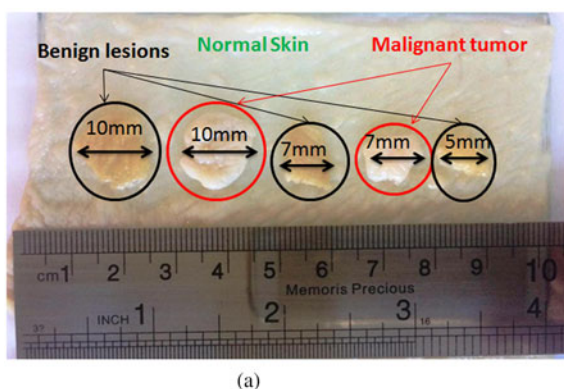


**Fig. 12.** (a) Artificial model to detect skin cancer at the early stage. (b) Magnitude of  $S_{11}$  and frequency shift ( $\Delta f$ ).

**Acknowledgments.** The Authors would like to thank the research laboratory of Faculty of Electrical and Computer Engineering at University of Sistan and Baluchestan for providing the laboratory facilities.

## References

1. Gu S et al. (2017) Broadband non-contact characterization of epitaxial graphene by near-field microwave microscopy. *Nanotechnology* **28**, 335702–335713.
2. Kim TH, James R and Narayanan RM (2017) High-resolution non-destructive testing of multilayer dielectric materials using wideband microwave synthetic aperture radar imaging. SPIE Conference on Nondestructive Characterization and Monitoring of Advanced Materials, Aerospace, and Civil Infrastructure 2017, Portland, 19 April 2017.
3. James R, Kim TH and Narayanan RM (2017) Prognostic investigation of galvanic corrosion precursors in aircraft structures and their detection strategy. SPIE Conference on Nondestructive Characterization and Monitoring of Advanced Materials, Aerospace, and Civil Infrastructure 2017, Portland, 19 April 2017.
4. Malyuskin O and Fusco V (2017) Super-resolution defect characterization using microwave near-field resonance reflectometry and cross-correlation image processing. *Sensing and Imaging* **18**, 7–18.
5. Ivashov S et al. (2016) High resolution MW holographic system for NDT of dielectric materials and details. 2016 16th International Conference on Ground Penetrating Radar (GPR), Hong Kong, pp. 1–5.
6. Nerguiziana V et al. (2017) Characterization of several cancer cell lines at microwave frequencies. *Measurement* **109**, 354–358.
7. Arkhyova K et al. (2017) Microwave dielectrometry as a tool for the characterization of blood cell membrane activity for in vitro diagnostics. *International Journal of Microwave and Wireless Technologies* **9**, 1569–1574.
8. Lin T, Gu S and Lasri T (2017) Highly sensitive characterization of glucose aqueous solution with low concentration: application to broadband dielectric spectroscopy. *Sensors and Actuators A: Physical* **267**, 318–326.
9. Cataldo A et al. (2017) TDR-based monitoring of rising damp through the embedding of wire-like sensing elements in building structures. *Measurement* **98**, 355–360.
10. Zhao R et al. (2017) The testing scheme for steel corrosion in the reinforced concrete via near field effect of meter-band wave. *Progress In Electromagnetics Research Letters* **66**, 127–134.
11. Zoughi R (2000) *Microwave Non-Destructive Testing and Evaluation Principles*. Norwell, MA, USA: Kluwer.
12. Malyuskin O and Fusco V (2016) High-resolution microwave near-field surface imaging using resonance probes. *IEEE Transactions on Instrumentation and Measurement* **65**, 189–200.
13. Haddadi K and Lasri T (2014) Geometrical optics-based model for dielectric constant and loss tangent free-space measurement. *IEEE Transactions on Instrumentation and Measurement* **63**, 1818–1823.
14. Haddadi K et al. (2011) Performance of a compact dual six-port millimeter-wave network analyzer. *IEEE Transactions on Instrumentation and Measurement* **60**, 3207–3321.
15. Bucci OM et al. (2017) Towards the assessment of detection limits in magnetic nanoparticle enhanced microwave imaging of breast cancer, Antennas and Propagation (EUCAP), 2017 11th European Conference, 19–24 March 2017.
16. Sugumaran S et al. (2018) Nanostructured materials with plasmonic nanobiosensors for early cancer detection: a past and future prospect. *Biosensors and Bioelectronics* **100**, 361–373.
17. Koutsoupidou M et al. (2017) Evaluation of a tumor detection microwave system with a realistic breast phantom. *Microwave and Optical Letters* **59**, 6–10.
18. Mirbeik-Sabzevari A, Ashinoff R and Tavassolian N (2017) Ultra-wideband millimeter-wave dielectric characteristics of freshly-excised normal and malignant human skin tissues. *IEEE Transactions on Biomedical Engineering* **99**, 1–11.
19. Khokhar U et al. (2017) Near-field tapered waveguide probe operating at millimeter waves for skin cancer detection, 2017 IEEE International Symposium on Antennas and Propagation & USNC/URSI National Radio Science Meeting, San Diego, CA.
20. Gao Y and Zoughi R (2017) Millimeter wave reflectometry and imaging for noninvasive diagnosis of skin burn injuries. *IEEE Transactions on Instrumentation and Measurement* **66**, 77–84.
21. Ghavami N et al. (2016) Huygens principle based UWB microwave imaging method for skin cancer detection. *Communication Systems, Networks and Digital Signal Processing (CSNDSP)*, 2016 10th International Symposium, Prague, Czech Republic, 20–22 July 2016.
22. Mehta P et al. (2006) Microwave reflectometry as a novel diagnostic tool for detection of skin cancers. *IEEE Transactions on Instrumentation and Measurement* **55**, 1309–1316.
23. Töpfer F, Dudorov S and Oberhammer J (2012) Micromachined 100 GHz near-field measurement probe for high-resolution microwave skin-cancer diagnosis. *IEEE/MTT-S International Microwave Symposium Digest*.
24. Taeb A, Gigoyan S and Safavi-Naeini S (2013) Millimetre-wave waveguide reflectometers for early detection of skin cancer. *IET Microwaves, Antennas & Propagation* **7**, 1182–1186.
25. Joines WT, Liu QH and Ybarra GA (2005) *Handbook of Biological Effects of Electromagnetic Fields*. Boca Raton, FL: CRC Press, 2005.
26. Topfer F and Oberhammer J (2015) Millimeter-wave tissue diagnosis: the most promising fields for medical applications. *IEEE Microwave Magazine* **16**, 97–113.
27. Sunteff V and Carruthers C (1946) The water content in the epidermis of mice undergoing carcinogenesis by methylcholanthrene. *Cancer Research* **6**, 574–577.
28. Zoughi R (2000) *Microwave Non-Destructive Testing and Evaluation*. The Netherlands: Kluwer Academic Publishers, Vol. 4, pp. 209–238.
29. Pozar DM (2012) *Microwave Engineering*, 4th Edn. New York: John Wiley.
30. Tabib-Azar M, Katz JL and LeClair SR (1999) Evanescent microwaves: a novel super-resolution noncontact nondestructive imaging technique for biological applications. *IEEE Transactions on Instrumentation and Measurement* **48**, 1111–1116.
31. Tabib-Azar M et al. (1999) Novel physical sensors using evanescent microwave probes. *Review of Scientific Instruments* **70**, 3381–3386.
32. Chen LF et al. (2004) *Microwave Electronics Measurement and Materials Characterization*. Chichester: John Wiley & Sons Ltd.
33. Gabriel S, Lau RW and Gabriel C (1996) The dielectric properties of biological tissues; III. Parametric models for the dielectric spectrum of tissues. *Physics in Medicine and Biology* **41**, 2271–2293.
34. Thompson RH et al. (2009) Tumor size is associated with malignant potential in renal cell carcinoma. *The Journal of Urology* **181**, 2033–2036.
35. Gniadecka M et al. (2004) Melanoma diagnosis by Raman spectroscopy and neural networks: structure alterations in proteins and lipids in intact cancer tissue. *Journal of Investigative Dermatology* **122**, 443.



and its applications.



**Fatemeh Kazemi** was born in Zahedan, Iran. She received the B.Sc. and M.Sc. degrees in Electrical Engineering from the University of Sistan and Baluchestan in 2005 and 2010, respectively. She is currently working toward the Ph.D. degree at the University of Sistan and Baluchestan, Zahedan, Iran. Her research concerns include microwave imaging, analysis and design of near-field probes, subsurface imaging

**Farahnaz Mohanna** received the B.Sc. degree in Electronics Engineering, from the University of Sistan and Baluchestan, Zahedan, Iran in 1987, and the M.Sc. degree in Electronics Engineering from the University of Tehran, Tehran, Iran in 1992, and the Ph.D. degree in Image Processing from the University of Surrey, Guildford, UK in 2002. She continued working as a research fellow at the Centre for Vision, Speech and Signal Processing (CVSSP) at the Surrey University, UK in 2003. She is currently an assistant professor at the University of Sistan and Baluchestan. Her research interests include communications, medical imaging, image processing, and computer vision.





**Javad Ahmadi-Shokouh** received the B.Sc. degree in Electrical Engineering from Ferdowsi University of Mashhad, Mashhad, Iran in 1993, the M.Sc. degree in Electrical Engineering from the University of Tehran, Tehran, Iran in 1995, and the Ph.D. degree in Electrical Engineering from the University of Waterloo, Waterloo, ON, Canada in 2008. He was also with the Department of Electrical Engineering, University of Manitoba, Winnipeg, MB, Canada (2008–2009)

as a postdoctoral fellow. He is currently an associate professor at the University of Sistan and Baluchestan. His research interests are antenna and microwave systems for all applications, millimeter-wave, smart antennas, and microwave imaging.